Soft Matter

PAPER

View Article Online
View Journal | View Issue

Published on 04 December 2013. Downloaded by McMaster University on 27/10/2014 15:14:02.

Cite this: *Soft Matter*, 2014, **10**, 1823

Polymer directed aggregation and dispersion of anisotropic nanoparticles

Tarak K. Patra and Jayant K. Singh*

The aggregation and dispersion of two anisotropic nanoparticles (NPs), cubes and tetrahedrons, in a polymer matrix are studied in this work using coarse-grained molecular dynamics simulations. We present the phase diagrams of NP–polymer composites, depicting microscopically phase-separated, dispersed, and bridged cubes and tetrahedrons in a polymer matrix, which depend on the interaction between the NPs and polymer (ε_{np}), along with the NPs' volume fraction (ϕ). The microscopic phase separation occurs at very low ε_{np}, where NPs self-organize into multidimensional structures, depending on ϕ. In particular, for tetrahedrons, a cross-over from an ordered spherical aggregate to a disordered sheet-like aggregate is observed with increasing ϕ. In the case of cubes, a transition from cubic array → square column → square array (sheet) is identified with increasing ϕ. The clusters of NPs are characterized by their asphericity and principal radii of gyration. The free energy profile for a structured assembly is estimated, which clearly shows that the successful assembly of NPs is energetically favorable at a lower temperature. However, there exists an energy barrier for the successful assembly of all the NPs in the system. At intermediate ε_{np}, a transition from a clustered state to a state comprising dispersed cubes and tetrahedrons in a polymer matrix is observed. At higher ε_{np}, a further transition takes place, where gas-like dispersed NPs form a liquid-like aggregate *via* polymer layers. Therefore, the findings in this work illustrate that the effective interaction between anisotropic NPs in a polymer matrix is very diverse, which can generate multidimensional structured assemblies, with the disordered clustering, dispersion, and bridging-induced aggregation of NPs.

Received 18th August 2013
Accepted 3rd December 2013

DOI: 10.1039/c3sm52216d

www.rsc.org/softmatter

I. Introduction

Polymer materials are attractive hosts that can control the morphology of nanoparticles (NPs), and generate ordered and hierarchical NP structures.[1–3] The optical, electrical, mechanical, and rheological properties of NP–polymer composite materials also change dramatically, which is largely due to the spatial distribution of NPs in the polymer matrix.[4–6] A remarkable variety of NPs (cubes, rods, tetrahedrons, tetrapods, *etc.*) are being synthesized, and are of great importance in nanotechnological applications such as photonics, electronics, energy storage devices, and biological sensors.[7,8] Among these anisotropic building blocks, cubes and tetrahedrons are faceted polyhedrals that have preferred symmetries for two-dimensional (2D) and three-dimensional (3D) packing. Therefore, the controlled self-assembly of these anisotropic particles can exploit their electrical, optical, and catalytic properties.[9] The fabrication of ordered assemblies of such asymmetric NPs is a great challenge because it is very sensitive to the thermodynamic and chemical conditions.[10] Polyhedral shapes are also found in certain viruses,[11] and in nanoscale building blocks such as the polyhedral oligomeric silsesquioxane (POSS) contained in nanoporous structures.[12] Therefore, the structural properties of faceted particles are of fundamental research interest. The variety of interactions present in polymer–NP solutions can be exploited to arrange NPs into ordered structures.[3] The depletion attraction between solvophobic particles induces microscopic phase separation in a polymer–NP solution, and it leads to the clustering of NPs, which do not mix with the polymer chains.[3,13–15] Spherical NPs, functionalized with polymeric tethers attached to specific locations on their surfaces, form spherical and cylindrical micelles along with a by-layer owing to depletion forces.[2,14,16] Similarly, tethered nanorods self-assemble into spherical and cylindrical micelles, depending on the nanorod volume fraction.[15,17] Tethered cubes have also been found to assemble into square columnar structures.[12] The tethered chains prevent the coalescence of adjacent clusters to form a larger aggregate. Therefore, a periodic array of such clusters forms in a polymer matrix.

The effective force between NPs is very important to understand these diverse structures. Qin and Fichthorn measured the solvation force between two NPs, immersed in a Lennard-Jones (LJ) liquid.[18] The solvation force is found to oscillate between attraction and repulsion as the separation between two solvophilic particles increases. However, the solvation force is always attractive when the particles are solvophobic.

Department of Chemical Engineering, Indian Institute of Technology Kanpur, Kanpur-208016, India. E-mail: jayantks@iitk.ac.in

Published on 04 December 2013. Downloaded by McMaster University on 27/10/2014 15:14:02.

Furthermore, the force between NPs has been found to depend on the adsorption of polymer on their surfaces,[19] polymer chain length,[20] and NP–polymer interaction strength,[22–24] which was also shown in our recent work.[21] Further, we observed that, at low NP–polymer interaction strengths, the effective interaction between NPs is very strong, leading to the clustering of spherical NPs. At intermediate NP–polymer interaction strengths, a very weak effective interaction between NPs leads to their dispersion. However, at a high NP–polymer interaction strength, the range of the effective interaction between NPs increases, allowing the bridging of NPs *via* polymer layers. In another study, Meng *et al.* showed that a cluster of spherical NPs in a polymer melt forms an apparently face-centered cubic (fcc) structure, and there is no self-assembly of NPs, whereas the cluster appears to be liquid-like in a monomer melt.[25] In contrast, the clustering of icosahedrons in a polymer melt is due to the self-organization of NPs.[26] Moreover, non-spherical particles such as hard tetrahedrons can pack more densely than spheres because of their preference for face-to-face alignment.[27,28] Tetrahedrons with truncated corners, on the other hand, are found not to align face-to-face, but form 2D sheets and one-dimensional (1D) chain structures because of the combination of electrostatic interaction and hydrophobic attraction between them.[29] Isotropic particles prefer to adopt a very compact packing such as an fcc or a hexagonal close pack (hcp) structure over a simple cube (sc) because they are energetically favorable, and the packing density is very low for sc. However, for cubic particles, it has been shown that the sc arrangement is more favorable energetically, as seen for iron oxide nanocubes, which prefer a face-to-face alignment with a 2D square lattice on a substrate [30] and an sc arrangement in bulk.[31] In addition, dipolar nanocubes self-assemble into a straight string and ring (1D).[32] Therefore, it is very important to understand the alignment and packing of such asymmetric particles, particularly when the particles assemble in a solution.

Apart from microscopic phase separation, at intermediate polymer–NP attraction strengths, the NPs disperse in the polymer matrix. The transition from the aggregate state to the dispersed state for spherical NPs is projected to be a first-order fluid–solid type transition.[25] On the other hand, this is not observed in the case of icosahedrons.[26] At higher interaction strengths, the bridging of NPs *via* polymer layers prevents their dispersion, which significantly affects the transport properties.[21,23,33,34] Though numerous studies have been done on NP–polymer systems, the clustering and phase transition of NPs in a polymer matrix are still poorly understood, and the following questions are very relevant. How does the self-assembly depend on the shape of the NPs? How are the ordered/disordered structures modified with an increase in the volume fraction of NPs? Is there any critical size for an NP cluster, beyond which the ordering breaks? Further, is the growth of the cluster always isotopic? Is 1D or 2D growth possible? What is the mechanism for the alignment of faceted particles in a polymer solution? Our motivation, in this work, is to address some of the above questions by considering tetrahedrons and cubes in a polymer melt using molecular dynamics (MD) simulations. We investigate self-assembled NPs' structures and their stability in relation to the depletion interaction at a weak NP–polymer interaction strength. Further, we study the dispersion and bridging of cubes and tetrahedrons at intermediate and higher NP–polymer interaction strengths, respectively. Finally, we present phase diagrams that summarize all the possible transitions in cube–polymer and tetrahedron–polymer systems.

The rest of this paper is organized as follows: models of the cube, tetrahedron, and polymer are presented in Section II. In addition, the simulation methodology is presented in Section II. In Section III, we discuss the results for both cube–polymer and tetrahedron–polymer systems. Finally, the conclusions are described in Section IV.

II. Model and method

The polymer is modeled as a linear chain of beads that are chemically identical. The beads interact through the Lennard-Jones (LJ) potential of the form

$$V(r) = 4\varepsilon\left[\left(\frac{r}{\sigma}\right)^{12} - \left(\frac{r}{\sigma}\right)^{6}\right] - V(r_c) \quad (1)$$

where ε and σ are the characteristic energy and length scale, respectively. All calculations are performed in reduced units, where ε, σ, and m are the characteristic energy, length, and mass parameters, respectively. The cut-off distances (r_c) are considered to be $2 \times 2^{1/6}\sigma$. In addition, the pairs of adjacent beads in all the chains are connected through the finitely extensible nonlinear elastic (FENE) potential,[35]

$$V_{FENE} = -0.5kR_0^2 \ln\left[1 - \left(\frac{r}{R_0}\right)^2\right] \quad (2)$$

where $R_0 = 1.5\sigma$ (finite extensibility) and $k = 30\varepsilon/\sigma^2$ (spring constant). $V_{FENE} = \infty$ when $r \geq R_0$.

We use a coarse-grained model to represent the NPs. One NP contains several coarse-grained beads frozen on its surface. These beads are placed on triangular lattice sites to create tetrahedron-shaped NPs, and on square lattice sites to create cubic NPs.[36] Schematic representations of the model NPs are shown in Fig. 1. The size and mass of each bead are represented by σ and m, respectively, which are identical to those of a polymer chain bead. A tetrahedron of edge length 5σ consists of 34 beads, and a cube of edge length 5σ consists of 98 beads. Any pair of beads from two different NPs interacts through the Weeks–Chandler–Andersen (WCA) potential, *i.e.*, eqn (1) with $r_c = 2^{1/6}\sigma$

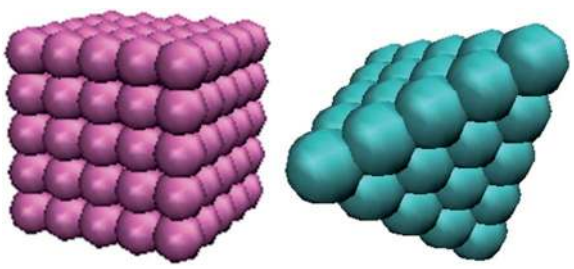

Fig. 1 The model NPs studied in this work. The NPs consist of coarse-grained beads on the outer surface of the particles. The cube consists of 98 beads, and the tetrahedron consists of 34 beads.

This journal is © The Royal Society of Chemistry 2014

Published on 04 December 2013. Downloaded by McMaster University on 27/10/2014 15:14:02.

and interaction strength $\varepsilon_{nn} = \varepsilon$. The beads in the same NP do not interact. The interaction between a bead of a NP and a monomer unit of a chain is attractive in nature and represented by eqn (1), with $r_c = 2.5\sigma$, and the strength of the interaction is ε_{np}. A polymer chain consists of 30 beads, and a total of 800 polymer chains are considered. Keeping the number of polymer chains unchanged, the number of NPs is varied from 8 to 100 to change the NPs' volume fraction. The temperature and pressure are reduced as $T^* = Tk_B/\varepsilon$ and $P^* = P\sigma^3/\varepsilon$, respectively. Here, k_B is the Boltzmann's constant. The system is periodic in all three directions. The equations of motions are integrated using the velocity Verlet algorithm,[37] with time step $\Delta t = 0.001\tau$. Here, $\tau = (\varepsilon/m\sigma^2)^{1/2}$ is the unit of time. At each time step, frozen subunits of a NP move together as a rigid body.[38] Initially, the MD simulations are performed in the isothermal-isobaric (NPT) ensemble at $P^* = 0.0$ and $T^* = 1.0$ for 10^8 time steps, which generate an equilibrium configuration for the system. The temperature and pressure are maintained by using a Nose–Hoover thermostat and barostat, respectively. Zero pressure is chosen to match the experimentally used atmospheric conditions.[22,24,39,40] The equilibrium simulations are long enough to allow each of the polymer chains to move a distance that is at least twice its radius of gyration.[41] The system is then simulated in the canonical (NVT) ensemble for a production run for another 10^8 time steps. The simulations are performed using LAMMPS (Large-scale Atomic/Molecular Massively Parallel Simulator).[42]

III. Results and discussion

The spatial distribution of NPs in a polymer matrix largely depends on the polymer–NP interaction, which is being explored in this study using various interfacial strengths, ε_{np}. Here, we present the results in two different subsections. In Section A, the self-assembly of NPs at weak interaction strengths is discussed, and the dispersion and bridging of NPs, which are observed at intermediate and high interaction strengths, respectively, are presented in Section B.

A. Self-assembly

The NPs are seen to self-assemble when the NP–polymer interaction strength $\varepsilon_{np} = 0.1$. At this weak interaction, the NPs and polymer microscopically phase separate because of the so-called entropic depletion interaction.[43,44] Fig. 2 shows the NP–NP radial distribution function (RDF) at $\varepsilon_{np} = 0.1$, which is defined as

$$g(r) = \frac{\langle N(r, r + \Delta r)\rangle}{\rho^* 4\pi r^2 \Delta r}. \quad (3)$$

Here, $\langle N(r,r + \Delta r)\rangle$ is the average number of particles in a spherical shell between distances r and $r + \Delta r$ from the center of mass (CM) of a particle. RDF represents the ratio of the average particle density in a shell of width Δr at a distance r from the CM of a particle to the bulk density (ρ^*) of the NPs in a given system. Fig. 2a presents the RDFs at different volume fractions for the case of tetrahedrons. The RDFs for volume fraction $\phi = 0.010$ and $\phi = 0.019$ correspond to sphere-like aggregations, and the RDF for $\phi = 0.024$ corresponds to a sheet-like

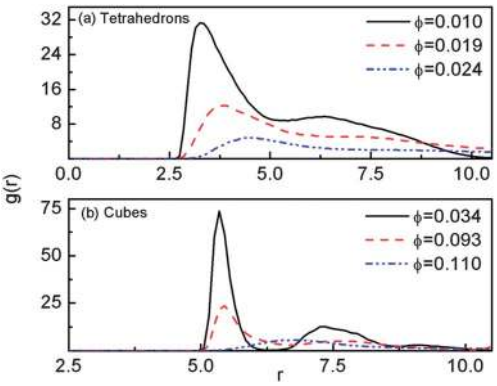

Fig. 2 The NP–NP RDF ($g(r)$). (a) corresponds to tetrahedrons, and (b) corresponds to cubes.

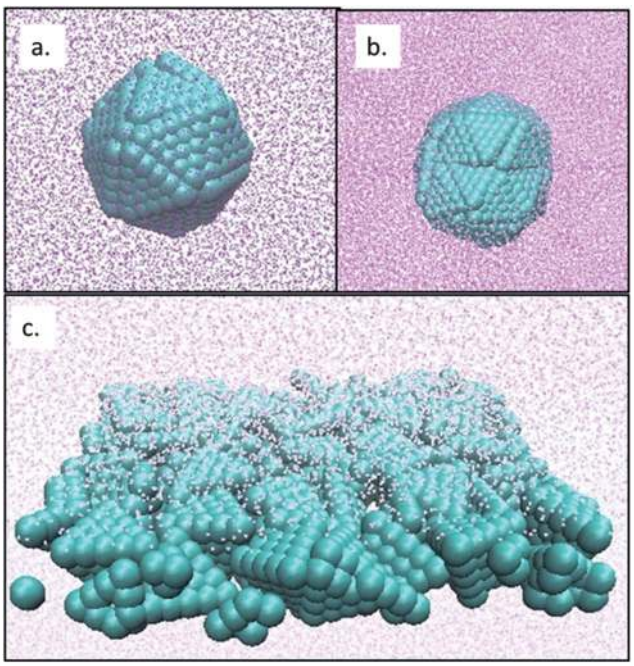

Fig. 3 MD snapshots of the assembled structures of tetrahedrons in a polymer melt. Assemblies of 20, 40 and 60 tetrahedrons are represented in a, b and c respectively. a, b and c correspond to volume fraction $\phi = 0.010$, $\phi = 0.019$, and $\phi = 0.024$, respectively.

aggregation. The corresponding MD snapshots are shown in Fig. 3a–c, respectively. The first non-zero value of RDF is found at approximately $r = 2.8\sigma$, which is the distance between the CMs of two particles when they are in face-to-face contact. As the particles' volume fraction increases, the position of the first peak shifts toward the right, which indicates an increase in the inter-particle separation distance. At $\phi = 0.024$, the peak height also decreases significantly, which suggests a decrease in the local particle density, where the aggregate becomes a sheet-like structure, as seen in Fig. 3c. Therefore, at this volume fraction, there is a cross-over from a 3D sphere-like aggregate to a 2D sheet-like aggregate. In the sheet-like aggregate, the tetrahedrons are not aligned face-to-face, and it is amorphous in nature. However, cubes are aligned face-to-face and ordered

Published on 04 December 2013. Downloaded by McMaster University on 27/10/2014 15:14:02.

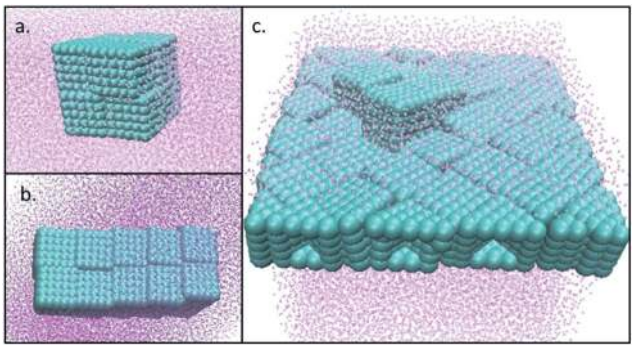

Fig. 4 MD snapshots of the assembled structures of cubes in a polymer melt. Assemblies of 8, 20 and 35 cubes are represented in a, b and c respectively. a, b and c correspond to volume fraction $\phi = 0.034$, $\phi = 0.093$, and $\phi = 0.110$, respectively.

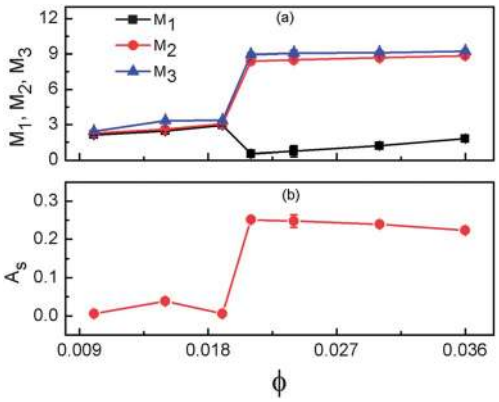

Fig. 5 (a) The principal radii of gyration of the cluster of tetrahedrons at different volume fractions. (b) The asphericity of the structure at different volume fractions.

self-assemblies are observed for the range of ϕ considered in this study. Here, we present the results for the range of ϕ where structural transitions take place. Fig. 2b shows the RDFs of cubic NPs at $\phi = 0.034$, $\phi = 0.093$, and $\phi = 0.110$. The corresponding MD snapshots are presented in Fig. 4a–c, respectively. The first non-zero value of RDF appears at approximately $r = 5\sigma$, which is the edge length of a cube representing the contact aggregation of NPs. The maximum RDF peak is found at $\phi = 0.034$, where a cubic arrangement of NPs is observed, as seen in the MD snapshot in Fig. 4a. The cubic arrangement of NPs transforms into a square column structure at $\phi = 0.093$. One block of the column consists of four cubes, as shown in Fig. 4b. With a further increase in ϕ, the columnar structure transforms into a sheet-like structure, which is a square array of NPs, as shown in Fig. 4c. This sheet of NPs forms at $\phi = 0.110$, where the first peak of the RDF is the lowest. All three structures have lattice symmetry. The NPs are arranged in a square array (in the 2D case) or a cubic array (in the 3D case), because these are energetically more favorable than a hexagonal arrangement.[30,31]

The shapes of the clusters, in this work, are characterized by their three principal radii of gyration and asphericity.[17,45] The principal radii of gyration of a cluster can be calculated from the square radius of a gyration tensor, defined as

$$R_{\gamma\beta}{}^2 = \left[\frac{1}{N}\sum_{i=1}^{N}(\gamma_i - \gamma_{cm})(\beta_i - \beta_{cm})\right], \quad (4)$$

where γ and β represent components of the position coordinates (x, y, and z) of the CM of a NP. γ_{cm} and β_{cm} are the components of position coordinates of the CM of a cluster (x_{cm}, y_{cm}, and z_{cm}). N is the number of NPs present in a cluster. The eigen values of the matrix are $R_1{}^2$, $R_2{}^2$, and $R_3{}^2$. Therefore, the three principal radii are $M_1 = \langle R_1{}^2\rangle^{1/2}$, $M_2 = \langle R_2{}^2\rangle^{1/2}$, and $M_3 = \langle R_3{}^2\rangle^{1/2}$. The asphericity of a cluster can be defined using the principal radii as

$$A_s = \frac{\sum_{i>j=1}^{3}\left(\langle R_i{}^2\rangle - \langle R_j{}^2\rangle\right)^2}{2\left(\sum_{i=1}^{3}\langle R_i{}^2\rangle\right)^2}. \quad (5)$$

Here, M_1, M_2, and M_3 are identical for a perfect sphere (3D). For an infinitely long, perfect cylinder (1D), the two principal radii are equal, and the third one is equal to infinity. On the other hand, one principal radius is finite, and the other two are infinite for an infinite sheet (2D). Hence, the asphericity values for a perfect sphere, cylinder, and sheet are 0.0, 0.5, and 0.25, respectively. The principal radii of gyration and asphericity of a cluster of tetrahedrons are shown in Fig. 5a and b, respectively. The value of A_s is close to 0.0 for $\phi \leq 0.019$, and changes to approximately 0.25 when $\phi > 0.019$. Similarly, the principal radii, M_1, M_2, and M_3, are of equal magnitude for $\phi \leq 0.019$, and two of them, M_2 and M_3, become very high for $\phi > 0.019$. Therefore, the principle radii and asphericity do not change for ϕ until 0.019, and a transition is clearly evident at approximately 0.021, where a sphere-like assembly becomes a sheet-like disordered structure. Fig. 6a and b presents the principal radii and asphericity, respectively, for the assembly of cubes at different ϕ. At $\phi = 0.034$, the particles assemble into a cubic structure, as seen in the MD snapshot of Fig. 2a. The asphericity is close to zero, and M_1, M_2, and M_3 are of equal magnitude. As the volume fraction increases, the cluster becomes a square

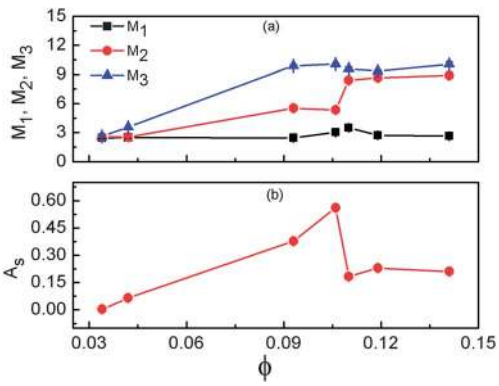

Fig. 6 (a) The principal radii of gyration of the cluster of cubes at different volume fractions. (b) The asphericity of the structure at different volume fractions. The size of error bar is smaller than symbol where it is not visible.

This journal is © The Royal Society of Chemistry 2014

Published on 04 December 2013. Downloaded by McMaster University on 27/10/2014 15:14:02.

column at $\phi = 0.093$. At this point, M_3 is significantly higher than M_1 and M_2, and the asphericity is also close to 0.5. This indicates the formation of a 1D structure, as seen in the MD snapshot (see Fig. 4b). A further increase in the NP volume fraction generates a sheet-like structure of cubes. At $\phi = 0.110$, the columnar structure becomes a sheet-like assembly, which is a square array of nanocubes. In this case, two principle radii, M_2 and M_3, are of equal magnitude, and significantly higher than M_1. The value of A_s drops to approximately 0.25, which is the ideal value for a 2D sheet. Therefore, the asphericity and principal radii of gyration identify two transition points: one at $\phi = 0.093$, where the 3D cubic array of nanocubes becomes a 1D square column, and another at $\phi = 0.110$, where the square column transforms into a 2D square array of nanocubes.

We infer that the tetrahedron cluster in the polymer melt grows from a sphere-like assembly to a sheet-like disordered aggregate as the NP volume fraction increases. This is in contrast to the behavior seen for nanocubes, where an ordered 1D columnar structure is observed between an ordered 3D cubic structure and a 2D sheet structure. No 1D structure is seen for the tetrahedral–polymer system. Hence, the transition from one structure to another is highly dependent on the shape of the NP.

To this end, we calculate the free energy landscape in order to understand the stability of such ordered structures and the assembly process. Two particles are perfectly assembled if they are aligned face-to-face, which can be measured, quantitatively, by the distance between their CMs and their orientation to each other. Following the work of Mahalik and Muthukumar,[11] we define a perfect assembly of size k as a cluster of k tetrahedrons, where all the adjacent particles in the cluster have a CM-to-CM distance of 2.8σ, and the alignment between them is 38°. The alignment is defined as the angle between the straight line that connects the CM and corner of one particle and the straight line that connects the CM and corner of another particle. Considering thermal fluctuation, we define an assembly as successful when each particle of a cluster has a maximum separation distance of $2.8\sigma + 0.5\sigma$ from its adjacent particles, and the alignment with its adjacent particles is within 38° + 5°. In the case of cubes, a structured assembly of size k is defined as a cluster of k cubes, where the maximum separation distance between each pair of adjacent cubes is $5\sigma + 0.5\sigma$, and the maximum alignment between them is 70° + 5°. Therefore, the NPs constitute a population of assembled structures, and the free energy of an assembled structure of size k can be written as[11]

$$F(k) = -k_B T \ln\left(\frac{kn_k}{\sum_{k=1}^{N} kn_k}\right), \quad (6)$$

with the reference state as $F(1) = 0.0$. Here, n_k is the number of assembled structures having size k. We next demonstrate the free energy landscape for a typical case of twenty NPs as a representation of the self-assembly process. Twenty tetrahedrons assemble into an icosahedron, and the corresponding volume fraction is 0.01. On the other hand, twenty cubes assemble into a square column, and the corresponding volume fraction is 0.093. The cluster distribution is calculated over data points collected for 10^8 simulation steps. Three independent simulations are carried out to determine the average landscape. The free energy landscape for the assembly of twenty tetrahedrons is shown in Fig. 7. At $T^* = 1.0$, the free energy of the cluster increases with its size, k. For the largest size, *i.e.*, $k = 20$, the free energy is $\sim 3.5k_BT$. Therefore, a successful assembly of twenty tetrahedrons is unfavorable by $\sim 3.5k_BT$. However, at a lower temperature, $T^* = 0.5$, the free energy first increases, with k reaching a maximum at $k = 10$. Subsequently, it decreases with a further increase in k, leading to a negative free energy value. Hence, at $T^* = 0.5$, the self-assembly process is favorable by $\sim -3k_BT$. The free energy landscape for the assembly of twenty cubes is similar to that seen for the tetrahedrons, as shown in Fig. 8. In this case, the successful assembly of twenty cubes is unfavorable by $\sim 7.0k_BT$ at $T^* = 1.0$. On the other hand, the process is favorable by $-1.5k_BT$ at $T^* = 0.5$. Therefore, to form an assembled cluster with twenty monomeric units at $T^* = 0.5$, an energy barrier needs to be overcome in both cases. As the process is favorable at $T^* = 0.5$, we infer that NPs have a strong

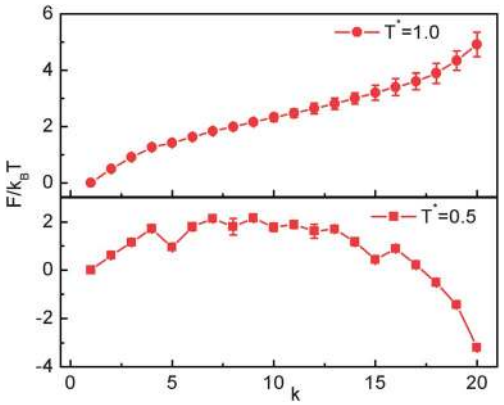

Fig. 7 The free energy landscape for the assembly of twenty tetrahedrons. The error bars represent the standard deviation of the free energy value from three independent simulations. The size of error bar is smaller than symbol where it is not visible.

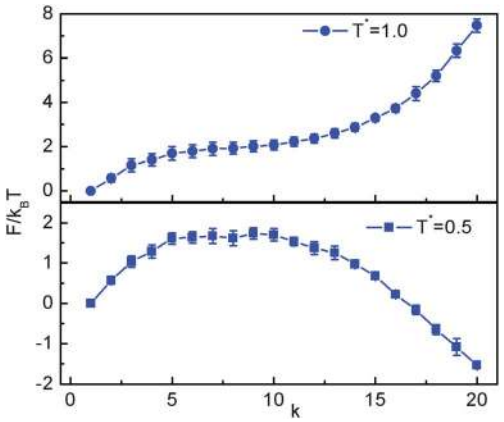

Fig. 8 The free energy landscape for the assembly of twenty cubes. The error bars represent the standard deviation of the free energy value from three independent simulations.

Published on 04 December 2013. Downloaded by McMaster University on 27/10/2014 15:14:02.

preference to assemble, and once it crosses the energy barrier, the cluster size grows until all the NPs are part of the cluster.

This self-assembly process has relevance in biophysical systems such as globular proteins, which can be crystallized by adding a non-adsorbing polymer to a protein solution;[46,47] in addition, a polymer plays an important role in the efficient self-assembly of mice viruses, which have a truncated tetrahedral shape.[11] The self-assembly of viral protein into icosahedral capsids has been shown to depend on the protein concentration and temperature, where the capsomers are added to the growing capsid at the downhill area of the free energy landscape.[48] Therefore, the observed self-assembly process that combines twenty tetrahedrons into an icosahedron resembles that of a virus assembly. This remarkable resemblance is very relevant to determine the correlations between the aggregation of biomolecules and the aggregation of inorganic NPs based on their similarity in shape.

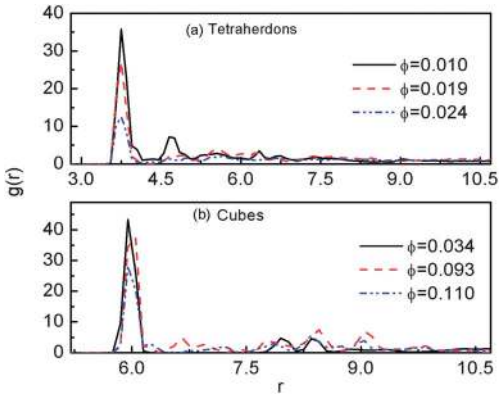

Fig. 10 The NP–NP RDF ($g(r)$) at $\varepsilon_{np} = 2.0$. (a) represents RDFs for tetrahedron–polymer system, and (b) represents cube–polymer system.

B. Dispersion and bridging

As the NP–polymer interaction strength increases, the structured assembly breaks, and the particles disperse throughout the system. The NP–NP RDFs at $\varepsilon_{np} = 0.8$ for both the tetrahedrons and cubes are shown in Fig. 9. Here, we present three case studies, for which the self-assembly results were presented in the previous section. Fig. 9a represents the RDF of the tetrahedrons in the polymer melt, and Fig. 9b shows that for the cubes in the polymer melt. In all three cases, the RDF increases to unity, which indicates that the NPs are in a gas-like state. Therefore, the particles are sterically stabilized in a polymer matrix, and are well dispersed in the matrix. The transition from microscopic phase separation to steric stabilization is driven by the entropy, similar to that observed for the case of spherical NPs.[21]

Notably, at $\varepsilon_{np} = 2.0$, NPs are bridged *via* polymer layers. Fig. 10a and b presents the NP–NP RDFs at $\varepsilon_{np} = 2.0$ corresponding to the tetrahedrons and cubes, respectively. In Fig. 10a, the first peak is found at approximately $r = 3.8\sigma$ for the tetrahedrons, and the CM–CM distance is 2.8σ when two tetrahedrons are in face-to-face contact. Therefore, this indicates that there is a polymer layer between a pair of tetrahedrons. At a higher volume fraction, the magnitude of the first peak decreases because of the increase in the bulk density, but the peak position remains unchanged. Similarly, for cubes (see Fig. 10b), the first peak is at $r = 6.0\sigma$, irrespective of the volume fraction, and the CM–CM distance is 5σ when two cubes are in face-to-face contact. Hence, this also indicates the existence of a polymer layer between a pair of cubes. Therefore, both systems reach the bridging state at $\varepsilon_{np} = 2.0$. The bridging induces the aggregation of NPs *via* a polymer layer, which is indicated by the large RDF peaks. The aggregation of particles can be explained as the dominance of energy over entropy, akin to that seen for spherical NPs.[21]

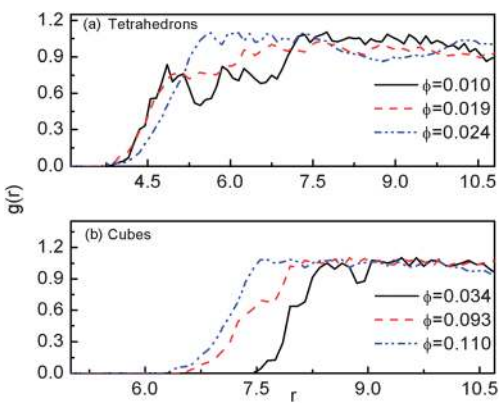

Fig. 9 The NP–NP RDF ($g(r)$) at $\varepsilon_{np} = 0.8$. (a) represents RDFs for tetrahedron–polymer system, and (b) represents cube–polymer system.

The transition from dispersion to the bridging-induced aggregation of NPs also has implications in biological systems. The aggregation and dispersion of bacteriorhodopsins, which are membrane proteins, have been found to be governed by lipid molecules.[49–52] The proteins aggregate in the presence of an annular lipid, which interacts very strongly with the protein, and no aggregation is observed in the presence of a neutral lipid, which interacts weakly with the protein.[51] Modeling the effective interaction between the proteins in lipid molecules as a square-well potential, Jagannathan *et al.* showed that the proteins have a monomeric form at a low value of the attractive well depth, whereas at moderate and high well-depth values, they are found to aggregate.[49] Therefore, the dispersion to aggregation behaviors of proteins, other biomolecules, and inorganic nanoparticles in a polymer matrix have similar characteristics, where the process is driven by the strong effective interaction between the fillers in the polymer matrix.

To elucidate the findings of Sections A and B, the phase diagrams are estimated, which represent all the possible spatial distributions of NPs in the ε_{np}–ϕ plane. Fig. 11 presents the phase diagram for the tetrahedron–polymer system. At a low ε_{np}, NPs form clusters for all the values of ϕ considered in this work. However, the shape of the cluster depends on ϕ. Two distinct clusters, ordered sphere-like and disordered sheet-like structures, are observed. The ordered assembly forms when $\phi \leq 0.023$, beyond which disordered clusters are generated, which is

 This journal is © The Royal Society of Chemistry 2014

Published on 04 December 2013. Downloaded by McMaster University on 27/10/2014 15:14:02.

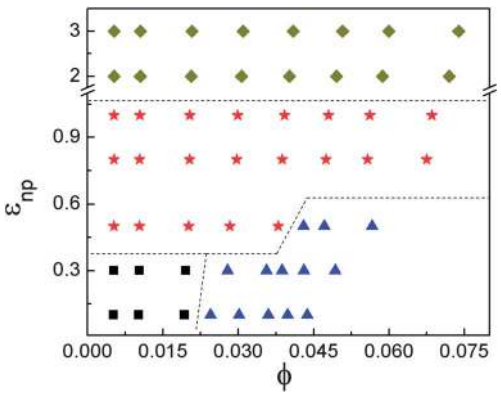

Fig. 11 The phase diagram representing all possible spatial distributions of tetrahedrons in the polymer matrix. ■: Sphere-like ordered structure, ▲: sheet like disordered structure, ★: dispersion, ◆: bridging of NPs *via* polymer layer. The dashed lines are to guide the eye, and are not thermodynamics boundaries.

evident from Fig. 11. As ε_{np} increases, the NPs disperse in the polymer matrix. However, at a higher volume fraction ($\varphi \geq 0.04$), the dispersed region dwindles, as the phase separation region exists for a wider range of NP–polymer interaction strengthens ($\varepsilon_{np} \leq 0.5$). When the NP–polymer interaction is sufficiently high ($\varepsilon_{np} \geq 2.0$), the NPs are bridged *via* polymer layers. Similarly, the phase diagram for the cube–polymer system is shown in Fig. 12. In this case, three ordered structures, namely a 3D cubic lattice, 1D square column, and 2D sheet structure form at a low NP–polymer interaction ($\varepsilon_{np} \leq 0.5$). A 1D square column structure is found between the 3D cubic and 2D sheet structures as φ increases. The dispersion of NPs is observed for $\varepsilon_{np} \geq 0.5$. The transition from dispersion to bridging depends on the volume fraction of the cubes in the polymer matrix. For a low volume fraction ($\phi \leq 0.1$), the bridging state is identified at $\varepsilon_{np} \geq 2.0$. However, for a high volume fraction ($\phi > 0.1$), bridging starts early at $\varepsilon_{np} \geq 0.8$. Hence the early bridging shrinks the dispersed region at a higher volume fraction.

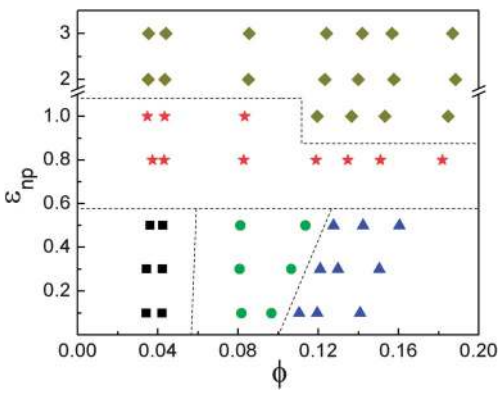

Fig. 12 The phase diagram representing all possible spatial distributions of cubes in the polymer matrix. ■: Cubic array assembly, ●: square column assembly ▲: sheet-like square array assembly, ★: dispersion, ◆: bridging of NPs *via* polymer layer. The dashed lines are to guide the eye, and are not thermodynamics boundaries.

IV. Conclusions

The spatial distribution of cubic and tetrahedron-shaped NPs was studied using coarse-grained MD simulations. This study mainly focused on the effects of polymer–NP interaction on the spatial arrangement of the NPs in a polymer matrix. At a very weak NP–polymer interaction strength, the polymer and the NPs microscopically phase separate because of the entropic depletion force. The depletion interaction force was utilized to assemble the NPs into well-defined structures. The principal radii of gyration and asphericity of the structures were calculated to analyze their shapes. When the NPs and polymers were microscopically phase separated, the cluster of NPs underwent a deformation with an increase in their volume fraction. Ordered and disordered clusters of NPs formed at low and high volume fractions of NPs, respectively, in the tetrahedron–polymer system, and we found structured assemblies of NPs with various shapes, depending on the NPs' volume fraction, in the cube–polymer system. The free energy landscape of an assembled cluster was estimated to understand its stability. The successful assembly of cubes and tetrahedrons at a lower temperature was found to be energetically favorable. However, in both cases, there was an energy barrier that needed to be overcome for the successful assembly of NPs. As the interaction strength increased, a transition from a clustered to a dispersed state occurred, where the NPs were sterically stabilized in a polymer matrix. A further increase in the interaction strength led to the aggregation of NPs *via* polymer layers. The phase diagrams were drawn to summarize the spatial arrangements of NPs in a polymer matrix. The microscopic phase separation, dispersion, and bridging of particles were found to depend not only on the NP–polymer interaction strength, but also on the NP volume fraction in the system. In particular, at a low NP–polymer interaction strength, $\varepsilon_{np} \leq 0.5$, three ordered structures, namely a 3D cubic lattice, 1D square column, and 2D sheet structure, formed in the cube–polymer system. This was in contrast to the case of the tetrahedron–polymer system, where two distinct clusters, ordered sphere-like and disordered sheet-like structures, were observed. At a higher NP–polymer interaction strength, the structural behaviors of the two systems were more or less alike.

This work demonstrated the important factors that govern the spatial arrangement of NPs in a polymer matrix. In particular, the depletion attraction is exploited to nucleate anisotropic particles into ordered structures, which is very important for the development of new materials and devices based on the ordered assembly of nanostructures. Further, the present study suggests that the dispersion of cubes and tetrahedrons in a polymer matrix can be achieved by controlling the NP–polymer interaction, which is necessary for optimizing the thermomechanical and electronic properties of NP–polymer composites.

Acknowledgements

This work is supported by the Department of Science and Technology (DST), Government of India. Computational resources are provided by the Centre for Development and Advance Computing (CDAC) Pune, India, and HPC cluster of the

Published on 04 December 2013. Downloaded by McMaster University on 27/10/2014 15:14:02.

Computer Center (CC), Indian Institute of Technology Kanpur. T. K. P. acknowledges the Council of Scientific and Industrial Research (CSIR), Government of India, for a senior research fellowship (SRF).

References

1 B. Gao, M. J. Rozin and A. R. Tao, *Nanoscale*, 2013, **5**, 5677.
2 P. Akcora, *et al.*, *Nat. Mater.*, 2009, **8**, 354.
3 D. Baranov, *et al.*, *Nano Lett.*, 2010, **10**, 743.
4 M. J. A. Hore and R. J. Composto, *Macromolecules*, 2012, **45**, 6078.
5 L.-T. Yan and X.-M. Xie, *Prog. Polym. Sci.*, 2013, **38**, 369.
6 S. K. Kumar, *et al.*, *Macromolecules*, 2013, **46**, 3199.
7 S. C. Glotzer and M. J. Solomon, *Nat. Mater.*, 2007, **6**, 557.
8 R. Taylor, *et al.*, *J. Appl. Phys.*, 2013, **113**, 011301.
9 F. Kim, *et al.*, *Angew. Chem., Int. Ed.*, 2004, **43**, 3673.
10 Y. Bai, *et al.*, *Powder Technol.*, 2012, **227**, 35.
11 J. P. Mahalik and M. Muthukumar, *J. Chem. Phys.*, 2012, **136**, 135101.
12 E. R. Chan, *et al.*, *Macromolecules*, 2005, **38**, 6168.
13 C. R. Iacovella, *et al.*, *Phys. Rev. E: Stat., Nonlinear, Soft Matter Phys.*, 2007, **75**, 040801(R).
14 Z. Zhang, *et al.*, *Nano Lett.*, 2003, **3**, 1341.
15 M. A. Horsch, Z. Zhang and S. C. Glotzer, *Phys. Rev. Lett.*, 2005, **95**, 056105.
16 J. R. Davis and A. Z. Panagiotopoulos, *J. Chem. Phys.*, 2008, **129**, 194706.
17 M. A. Horsch, Z. Zhang and S. C. Glotzer, *J. Chem. Phys.*, 2006, **125**, 184903.
18 Y. Qin and K. A. Fichthorn, *J. Chem. Phys.*, 2003, **119**, 9745.
19 K. T. Marla and J. C. Meredith, *Langmuir*, 2005, **21**, 487.
20 X. Z. Cao, *et al.*, *Phys. Rev. E: Stat., Nonlinear, Soft Matter Phys.*, 2011, **84**, 041802.
21 T. K. Patra and J. K. Singh, *J. Chem. Phys.*, 2013, **138**, 144901.
22 J. S. Smith, D. Bedrov and G. D. Smith, *Compos. Sci. Technol.*, 2003, **63**, 1599.
23 J. B. Hooper and K. S. Schweizer, *Macromolecules*, 2005, **38**, 8858.
24 J. Liu, *et al.*, *Langmuir*, 2011, **27**, 7926.
25 D. Meng, *et al.*, *Soft Matter*, 2013, **9**, 5417.
26 F. W. Starr, J. F. Douglas and S. C. Glotzer, *J. Chem. Phys.*, 2003, **119**, 1777.
27 P. F. Damasceno, M. Engel and S. C. Glotzer, *ACS Nano*, 2012, **6**, 609.
28 A. Haji-Akbari, *et al.*, *Nature*, 2009, **462**, 773.
29 Z. Tang, *et al.*, *Science*, 2006, **314**, 274.
30 S. Yamamuro and K. Sumiyama, *Chem. Phys. Lett.*, 2006, **418**, 166.
31 S. Yamamuro, K. Sumiyama and T. Kamiyama, *Appl. Phys. Lett.*, 2008, **92**, 113108.
32 X. Zhang, Z. Zhang and S. C. Glotzer, *J. Phys. Chem. C*, 2007, **111**, 4132.
33 J. B. Hooper and K. S. Schweizer, *Macromolecules*, 2006, **39**, 5133.
34 J. B. Hooper and K. S. Schweizer, *Macromolecules*, 2007, **40**, 6998.
35 G. S. Grest and K. Kremer, *Phys. Rev. A*, 1986, **33**, 3628.
36 A. Santos, J. A. Millan and S. C. Glotzer, *Nanoscale*, 2012, **4**, 2640.
37 M. P. Allen and D. J. Tildesley, *Computer Simulations of Liquids*, Clarendon, Oxford, 1987.
38 H. Kamberaj, R. J. Low and M. P. Neal, *J. Chem. Phys.*, 2005, **122**, 224114.
39 A. Chremos and A. Z. Panagiotopoulos, *Phys. Rev. Lett.*, 2011, **107**, 105503.
40 D. Bedrov, G. D. Smith and J. S. Smith, *J. Chem. Phys.*, 2003, **119**, 10438.
41 T. Desai, P. Keblinski and S. K. Kumar, *J. Chem. Phys.*, 2005, **122**, 134910.
42 S. J. Plimpton, *J. Comput. Phys.*, 1995, **117**, 1.
43 F. Oosawa and S. Asakura, *J. Chem. Phys.*, 1954, **22**, 1255.
44 A. Vrij, *Pure Appl. Chem.*, 1976, **48**, 471.
45 M. Kenward and M. D. Whitmore, *J. Chem. Phys.*, 2002, **116**, 3455.
46 A. M. Kulkarni, *et al.*, *J. Chem. Phys.*, 2000, **113**, 9863.
47 O. Galkin and P. G. Vekilov, *Proc. Natl. Acad. Sci. U. S. A.*, 2000, **97**, 6277.
48 H. D. Nguyen, V. S. Reddy and C. L. Brooks, *Nano Lett.*, 2007, **7**, 338.
49 K. Jagannathan, R. Chang and A. Yethiraj, *Biophys. J.*, 2002, **83**, 1902.
50 K. C. Ng and L. K. Chu, *J. Phys. Chem. B*, 2013, **117**, 6241.
51 M. C. Sabra, J. C. M. Uitdehaag and A. Watts, *Biophys. J.*, 1998, **75**, 1180.
52 A. Watts, *Biophys. Chem.*, 1995, **55**, 137.

 This journal is © The Royal Society of Chemistry 2014